

Helical spin-density wave in $V_{2-y}O_3$

T. Wolenski, M. Grodzicki, J. Appel
Universität Hamburg, I. Institut für Theoretische Physik
Jungiusstraße 9, D-20355 Hamburg.
(Submitted: November 6, 1997)

Recent neutron scattering and nuclear magnetic resonance experiments have revealed that the low temperature phase of doped $V_{2-y}O_3$ is an itinerant antiferromagnet with a helical spin structure. We use a band structure calculation as the point of departure to show that these experiments are in agreement with mean field results for an Overhauser spin-density wave state. The influences of a finite life-time and of dilute magnetic impurities are discussed.

I. INTRODUCTION

Stoichiometric V_2O_3 is generally considered a classic Mott-Hubbard system displaying a first order transition at $T_N=155$ K from a paramagnetic metal (PM) to a local-moment antiferromagnetic insulator (AFI). It is common wisdom that this transition is driven by the strong Coulomb interactions between conduction band electrons which opens up the Mott-Hubbard gap. The antiferromagnetism, which lifts the degeneracy in the insulating phase, is therefore a consequence of the interaction-driven opening of the gap between the upper and lower Hubbard band.

Experimentally the situation appears to be quite different in doped $V_{2-y}O_3$, where the low temperature phase is an antiferromagnetic metal (AFM) with an incommensurate Overhauser spin-density wave (SDW), similar to metallic chromium. Neutron scattering experiments¹ show that the SDW has a nesting vector $\mathbf{Q} = 1.70 c^*$ (c^* is a reciprocal lattice vector in the hexagonal unit cell of V_2O_3), and that the transition appears at a T_N of about 10 K; both T_N and \mathbf{Q} are almost independent of doping in the regime probed. The ordered moment is only $\mu = 0.14 \mu_B$ as compared to the $1.2 \mu_B$ in the AFI.

Moreover, the magnetic excitations are found² to have a bandwidth of about $20 k_B T_N$. In a local moment picture one would expect a magnetic bandwidth of order $J \sim k_B T_N$. The large bandwidth can be understood in the framework of SDW theory, where, however, excitations are found on electronic energy scales. An interesting observation is that even close to the metal-insulator transition the magnetic excitations correspond to the SDW spin structure rather than the magnetic order in the antiferromagnetic Mott insulator phase. This suggests³ that the local vanadium moment formation in the AFI phase is accompanied by a change in the electronic configuration.

NMR experiments by Langenbuch and Pieper⁴ have confirmed the neutron scattering results for the ordered moment of about $0.14 \mu_B$ and the orientation of the SDW along the c -direction. The magnitude of the local magnetic field is identical on all V-sites, compatible with a helical rather than linear polarization. At lower doping the temperature dependence of the spin-echo intensity also shows $T_N \simeq 10$ K. However, at doping $y \geq 0.038$ the transition observed with NMR shows $T_N \simeq 50$ K, with

no special feature in the V relaxation rate around 10 K. The phase diagram combining these experimental results is shown in Fig. 1. An additional important contribution of NMR is the study of the minority V sites neighboring the vanadium vacancies in c -direction. These sites are approximately in a V^{4+} ($S=1$) state. Furthermore, the 10 K transition could be intrinsic to the V_2O_3 system, while the magnetic impurities increase the transition temperature above a certain impurity concentration. We will discuss this scenario in Sec. V. The homogeneous susceptibility at higher doping⁴ is very sensitive to whether the measurement is made in zero field or in the presence of the earth magnetic field. In the former case, for $y=0.052$ a transition is seen at 56 K, while there is no feature at 10 K. In the latter case, there is only some hysteresis left at higher temperatures, while there is a pronounced peak at 10 K.

The order of the phase transition is an issue not completely settled by these experiments. While the neutron scattering data are consistent with a BCS-like second order transition at 10 K modified by fluctuations, the NMR data show, at least for the 50 K transition, a large discontinuity in the local magnetic field at T_N .

There have been attempts to qualitatively study the itinerant AFM phase using the LISA (local impurity self-consistent approximation) method starting from the limit of strong correlations⁵, where the key factor for the closing of the Hubbard gap is the magnetic frustration caused by the defect sites and the V^{4+} moments. However, as pointed out above, the experiments indicate a conventional Overhauser SDW resulting from Coulomb interactions at nested Fermi surface sheets. In this paper we show that it is possible to explain the experiments with a molecular-field Hartree-Fock SDW calculation starting from accurate band structure results and taking into account realistic electron-electron scattering and multiple bands at the Fermi level.

In the following section we discuss the band structure calculation, which is the point of departure for the Hartree-Fock SDW calculation with life-time effects discussed in Sec. III. The results will be discussed in Sec. IV. In Sec. V we compare our results with the NMR and neutron scattering experiments and discuss the importance of magnetic impurities.

II. BAND STRUCTURE

The first band structure calculations for V_2O_3 date back to the early seventies.⁶ However, at that time only a tight-binding calculation with a rather small set of orbitals was feasible. Recently, Mattheiss⁷ performed a state-of-the-art calculation using the scalar-relativistic linear augmented-plane-wave (LAPW) method. We make use of his results in the form of a Slater-Koster⁸ calculation using the parameters given by Mattheiss.

In the Slater-Koster method the band structure is constructed from parameters obtained at special points of high symmetry using LDA-APW results. Then, the energy eigenvalues at general \mathbf{k} are interpolated using a tight-binding-like formalism, thus preserving the full symmetry of the lattice.

To find the energy eigenvalues, in general one has to calculate integrals of the form

$$H_{\mu\mu'} = e^{i\mathbf{k}(\mathbf{R}_\mu - \mathbf{R}_{\mu'})} \int \phi_\mu^*(\mathbf{r} - \mathbf{R}_\mu) H \phi_{\mu'}(\mathbf{r} - \mathbf{R}_{\mu'}) d\mathbf{r} \quad (1)$$

for a Hamiltonian

$$H = T + \sum_{\kappa} V_{\kappa}(\mathbf{r} - \mathbf{R}_{\kappa}). \quad (2)$$

If μ , μ' and κ are all different, the integrals are three-center integrals; if $\kappa = \mu$ or $\kappa = \mu'$, they are two-center integrals. The three-center integrals tend to be smaller, and the angular dependence differs only for the $l > 0$ contribution, so that it is a good approximation to only consider two-center integrals (extended Hückel approximation). The wave functions ϕ and the potential V_{κ} are not very well known. Therefore, the concept of the Slater-Koster method is to treat the two-center integrals as parameters obtained from LDA calculations at special points, rather than calculate them microscopically. The remaining non-trivial task is to construct the full matrix elements between all 44 orbitals considered in the trigonal unit cell of V_2O_3 : Five $3d$ -orbitals for each of the four vanadium atoms and one $2s$ - and three $2p$ -orbitals for each of the six oxygen atoms in the unit cell.

In Fig. 2 we show the bands in a trigonal crystal structure plotted along lines of high symmetry. The symmetry points are labeled using the hexagonal notation, the Fermi energy is set to be zero. In Fig. 3 we plot the density of states in the vicinity of the Fermi energy, stemming predominantly from the $V(3d)$ -bands. We also plot the density of states from the two bands (labeled band A and B respectively) which contribute about 80 percent of the total density of states at the Fermi energy. Note that the densities of states of band A and band B at the Fermi energy are almost equal.

The Fermi surface is rather complicated, and therefore we restrict ourselves here to showing two cuts through the Brillouin zone: Fig. 4 a) is in the a - b ($k_z=0$) plane and reflects nicely the trigonal symmetry of the lattice: a three-fold rotation axis in c -direction combined with inversion symmetry around the origin. This symmetry leads to magnetic frustration in the a - b plane, in

agreement with the observed SDW nesting vector in c -direction. In Fig. 4 b) we show a second cut in the a - c ($k_y=0$) plane, where we indicated the main nesting feature of the Fermi surface with an arrow. The nesting vector has been calculated numerically from the maximum in the susceptibility (cf. Sec. IV), the arrow in this figure only serves for illustration purposes, in particular since the Fermi surface is truly three-dimensional and thus a single two-dimensional cut can be misleading. The nesting part of the Fermi surface we indicated extends into the b -direction, thus giving a sufficient density of states to produce a spin-density wave as will be shown in the next section.

Strictly, the band structure calculation is performed for stoichiometric V_2O_3 . However, the doping in the samples experimentally probed is sufficiently small ($y \leq 0.05$) that even at the highest doping levels the chemical potential is only shifted by a few meV, justifying a rigid band approximation.

III. HELICAL SPIN-DENSITY WAVE THEORY

A. Molecular-field gap equation

A helical spin-density wave instability, where electrons with momentum \mathbf{k} and holes with momentum $\mathbf{k}+\mathbf{Q}$ and opposite spins pair below a critical temperature and thus produce a gap at parts of the Fermi surface, has first been proposed by Overhauser⁹ for the Hartree-Fock electron gas. While for the three-dimensional electron gas this instability is prevented by screening, certain Fermi surface topologies with sizeable parallel parts of the Fermi surface connected by a single vector \mathbf{Q} (nesting) lead to the appearance of an SDW phase in actual materials like chromium.¹⁰

Starting from a Hubbard Hamiltonian

$$H = \sum_{\mathbf{k},\alpha} \epsilon_{\mathbf{k}} c_{\mathbf{k},\alpha}^{\dagger} c_{\mathbf{k},\alpha} + U \sum_{\mathbf{k},\mathbf{k}',\mathbf{q}} \sum_{\alpha,\alpha'} c_{\mathbf{k},\alpha}^{\dagger} c_{\mathbf{k}',\alpha'} c_{\mathbf{k}'-\mathbf{q},\alpha'} c_{\mathbf{k}+\mathbf{q},\alpha}, \quad (3)$$

the assumption of a finite expectation value for $S_{\mathbf{Q}}^{\uparrow\downarrow} = \sum_{\mathbf{k}} \langle c_{\mathbf{k}+\mathbf{Q}\uparrow}^{\dagger} \sigma_{\uparrow\downarrow}^z c_{\mathbf{k}\downarrow} \rangle$ in the Hartree-Fock approximation leads to a molecular-field equation for the SDW gap by means of a standard Bogoliubov transformation, rather similar to the BCS gap equation. Since the nesting vector \mathbf{Q} is determined by the Fermi surface topology, it will in general be incommensurate with the lattice. The gap equation has been generalized to the incommensurate situation by Young,¹¹ in our notation it reads

$$1 = \frac{U}{N} \sum_{\mathbf{k}} \frac{f(E_{\mathbf{k}}^+) - f(E_{\mathbf{k}}^-)}{\sqrt{(\epsilon_{\mathbf{k}} - \epsilon_{\mathbf{k}+\mathbf{Q}})^2 + 4\Delta^2}}. \quad (4)$$

The quasi-particle energies are given by

$$E_{\mathbf{k}}^{\pm} \equiv \frac{\epsilon_{\mathbf{k}} + \epsilon_{\mathbf{k}+\mathbf{Q}}}{2} \pm \frac{1}{2} \sqrt{(\epsilon_{\mathbf{k}} - \epsilon_{\mathbf{k}+\mathbf{Q}})^2 + 4\Delta^2}, \quad (5)$$

and $f(E) = 1/(\exp(E/k_B T) + 1)$ is the Fermi function.

The assumption of a finite expectation value $S_{\mathbf{Q}}^{\uparrow\downarrow}$ leads to a spiral polarization of the SDW,¹² as we can show from considering $S_{\mathbf{Q}}^+ = S_{\mathbf{Q}}^{\uparrow\downarrow} \equiv \bar{S}_{\mathbf{Q}}$ and $S_{-\mathbf{Q}}^- = S_{-\mathbf{Q}}^{\uparrow\downarrow} = \bar{S}_{\mathbf{Q}}^*$. As usual, they are related to S^x and S^y by $S^x = (S^+ + S^-)/2$ and $S^y = (S^+ - S^-)/2$. The Fourier transforms then are

$$\begin{aligned} S_{\mathbf{Q}}^x(\mathbf{R}) &= (S_{\mathbf{Q}}^+(\mathbf{R}) + S_{-\mathbf{Q}}^-(\mathbf{R}))/2 \\ &= \bar{S}_{\mathbf{Q}}(\exp(i\mathbf{Q} \cdot \mathbf{R}) + \exp(-i\mathbf{Q} \cdot \mathbf{R}))/2 \\ &= \bar{S}_{\mathbf{Q}} \cos \mathbf{Q} \cdot \mathbf{R} \end{aligned} \quad (6)$$

$$S_{\mathbf{Q}}^y(\mathbf{R}) = \bar{S}_{\mathbf{Q}} \sin \mathbf{Q} \cdot \mathbf{R}, \quad (7)$$

which is a spiral polarization. If the nesting instability were strong enough to simultaneously support an SDW with opposite helicity, we would get a linear polarization. In the present case, however, the subtle modification of the Fermi surface through the formation of one spiral SDW is sufficient to prevent this additional, opposite SDW.

B. Life-time effects due to quasiparticle scattering

The analysis we presented so far is for a one-band model without any scattering. As we show in the preceding section, at least two bands are relevant for the low energy physics of V_2O_3 . Testing the nesting properties of these two bands, it shows however, that only one of them shows significant nesting leading to a possible SDW instability. Hence, our approach is to assume that the SDW results from the nesting band A, while band B enters the physics via scattering processes from the part of the inter-band Coulomb interaction not already taken into account in the LDA band structure. Since the densities of states at the Fermi energy of bands A and B are comparable, this scattering is expected to significantly shorten the life-time of band A quasi-particles.

The scattering results from both electron-electron interactions, τ_{e-e}^{-1} , and the scattering of electrons from the vanadium vacancy sites, τ_{imp}^{-1} . The sizeable electron-electron scattering, which has the form¹³ (N_A and N_B are the densities of states for the respective bands)

$$\tau_{e-e}^{-1} = cN_A(0)N_B(0)(\pi^2(k_B T)^2 + (\hbar\omega)^2), \quad (8)$$

is responsible for the T^2 term in the electrical resistivity,¹⁴ while τ_{imp}^{-1} determines the residual resistivity at $T = 0$. We thus have

$$\tau^{-1} = cN_A(0)N_B(0)(\pi^2(k_B T)^2 + (\hbar\omega)^2) + \tau_{\text{imp}}^{-1}. \quad (9)$$

The constant c contains the scattering cross section. To estimate c we use the relation between resistivity and scattering rate,

$$\rho = \frac{m^*}{ne^2} \tau^{-1}. \quad (10)$$

The carrier density n can be estimated from the Hall coefficient,

$$R_H = \frac{1}{ne}. \quad (11)$$

Experimentally,¹⁵ $R_H = 3.5 \times 10^{-4} \text{ cm}^3 \text{ C}^{-1}$, resulting in a carrier density $n = 1.8 \times 10^{22} \text{ cm}^{-3}$. The coefficient of the T^2 term in the resistivity¹⁴ is $6.0 \times 10^{-8} \Omega \text{ cm K}^{-2}$. Taking all these values derived from different experiments at face value, a realistic effective mass m^* of a few times m results in a scattering rate $\hbar\tau^{-1}/k_B \simeq 10 \text{ K}$ at T_N . One should consider this an estimate of τ^{-1} , which serves to prove the consistency of our approach, rather than an exact value, and hence we will parameterize the scattering rate by multiplying with a scaling parameter α , which varies between 0.1 and 1, i.e.

$$\hbar\tau = \alpha(k_B T)^2. \quad (12)$$

To take these life-time effects into account we make use of an approach first applied to the case of BCS superconductors with strong damping of the quasi-particles by Bardasis and Schrieffer.¹⁶ These authors derive the molecular-field gap equation including the Nambu-Eliashberg function $Z(\mathbf{q}, \omega)$, which is related to the scattering rate τ^{-1} via

$$Z(\mathbf{k}, \omega) = \text{Re}Z(\mathbf{k}, \omega) \left(1 + i \frac{\tau^{-1}}{\omega} \right). \quad (13)$$

The real part of $Z(\mathbf{q}, \omega)$ renormalizes the band structure and is already taken into account in LDA. Thus, we set $\text{Re}Z(\mathbf{k}, \omega) = 1$. The imaginary part of $Z(\mathbf{q}, \omega)$ is taken into account by straightforward generalization of the gap equation of Ref. 16 to the case of an incommensurate SDW and to finite temperatures by employing the usual summation technique over Matsubara frequencies; one arrives at

$$\begin{aligned} 1 &= \frac{U}{N} \text{Re} \sum_{\mathbf{k}} \frac{f(E_{\mathbf{k}}^+) - f(E_{\mathbf{k}}^-)}{Z \sqrt{(\epsilon_{\mathbf{k}} - \epsilon_{\mathbf{k}+\mathbf{Q}})^2 + 4\Delta^2}} \times \\ &\times \left(1 - E_{\mathbf{k}} \frac{d}{d\omega} \frac{1}{Z} \Big|_{\omega=E_{\mathbf{k}}/Z} \right)^{-1}. \end{aligned} \quad (14)$$

IV. RESULTS

The necessary first step is to determine the nesting vector \mathbf{Q} . There are two basically equivalent ways to do this: One can examine the \mathbf{q} -dependent susceptibility

$$\chi^0(\mathbf{q}) = \sum_{\mathbf{k}} \frac{f(\epsilon_{\mathbf{k}+\mathbf{q}}) - f(\epsilon_{\mathbf{k}})}{\epsilon_{\mathbf{k}+\mathbf{q}} - \epsilon_{\mathbf{k}}} \quad (15)$$

and look for a maximum at a position \mathbf{q}_{max} . Within RPA, where the full susceptibility is given by $\chi_{\text{RPA}}(\mathbf{q}) = \chi^0(\mathbf{q})/(1 - U\chi^0(\mathbf{q}))$, with increasing U the phase transition will first occur for $\mathbf{Q} = \mathbf{q}_{\text{max}}$. Equivalently, one can study the gap equation Eq. (14), and calculate the value of \mathbf{q} that leads to the minimum value of U necessary to satisfy the gap equation at a given temperature, i.e. to

produce the SDW phase transition. Both methods lead to the same result $\mathbf{Q} = (1.69 \pm 0.03)c^*$ in surprisingly good agreement with the neutron scattering results.¹ In Fig. 5 we show the susceptibility plotted for different values of \mathbf{q} along the c -direction in the paramagnetic state close to the SDW transition.

Since the effective screened interaction U is not known very well from first principles, we use it as a parameter to fix T_N . From optical conductivity data¹⁷ U has been estimated to be about 1 eV, a value also used in the LISA calculations⁵. In Fig. 6 we plot the interaction U_c necessary to obtain a given critical temperature for the SDW transition.

The next step is to solve the gap equation for given U and τ for the SDW gap $\Delta(T)$. In Fig. 7 we show the results for a T_N of 10 K and different scattering rates. Clearly, the jump in the order parameter at T_N increases with increasing scattering rate. However, even at the lower limit of the reasonable range of scattering rates this discontinuity is significant, in agreement with the findings of Pieper *et al.*⁴.

There has been some discussion in the context of chromium as to how a mean-field SDW transition can become first order. One suggestion is the effect of a “reservoir band”,¹⁸ which is polarized by the formation of the SDW. Clearly, a strong coupling to the lattice will also enhance the tendency towards a first order transition. In the present case, however, the strong lifetime effects of our two-band model already produce a first order transition. The life-time effects are stronger for the 50 K transition than for the 10 K transition, so that it is possible that the 10 K transition is modified once fluctuations are taken into account.

It is hard to estimate the size of the ordered magnetic moment from this calculation, since we did not test the full \mathbf{q} -dependence of the order parameter. However, we calculated that about ten percent of the Fermi surface make the main contribution to the SDW instability, in agreement with an estimate of Bao *et al.*¹.

V. DISCUSSION AND CONCLUSIONS

Taking an LDA band structure calculation as point of departure, we find a SDW transition at 10 K with realistic parameters with a nesting vector $\mathbf{q}=1.69 c^*$ and a helical spin structure in agreement with neutron scattering results.¹ We believe that this SDW is the intrinsic low temperature phase of doped $V_{2-y}O_3$. This leaves the puzzle of the partial disagreement of neutron scattering and NMR⁴ as to what the transition temperature of the higher doped compounds is.

We suggest the following scenario for the higher doped compounds. The V site neighboring a vanadium vacancy in c -direction is in a V^{4+} state⁴ with $\mu = 1\mu_B$. These moments are very dilute at the relevant concentrations $y \leq .05$. Overhauser¹⁹ and recently Werner²⁰ have shown how an incipient SDW combined with magnetic impurities can lead to an SDW transition. The SDW is driven by the maximization of the interaction

energy $E_{\text{int}} = \mathbf{H}_j \cdot \mathbf{S}_j$, where \mathbf{H}_j is the local field due to the SDW and \mathbf{S}_j the impurity spin. If the RKKY-type interactions between the dilute impurities are strong enough, this mechanism will also lead to the formation of a domain structure, which could explain the difference between neutron scattering and the more local NMR experiments.

An open question is whether the delicate field dependence in the experiments of Pieper *et al.*⁴ is related to an ordering of the V^{4+} moments, preventing the formation of helical SDW domains. Problematic is that the critical field, which would have to overcome the RKKY interaction between the dilute moments, is only of the order of 1 G. It is known that strong non-linearities exist in spin glass systems,²¹ where comparable fields are sufficient to suppress a sharp cusp in the susceptibility. However, this point clearly requires further attention, to clarify the experimental findings.

Another open question is how the Mott transition at 155 K, which apparently is accompanied by a change in the electronic configuration—and also in the lattice symmetry, which becomes monoclinic in the AFI insulator—is influenced by taking into account the realistic multi-band bandstructure. Particularly the intriguing experimental observation, that the fluctuations on the metallic side of the metal-insulator type are of the SDW rather than local moment type with a magnetic structure given by Fermi surface topology, show that for the physics of the Mott transition in V_2O_3 both strong correlation and electronic structure effects are important. This problem is under investigation.

ACKNOWLEDGMENTS

We like to thank M. W. Pieper for insightful discussions. T. W. acknowledges financial support through a fellowship from the Universität Hamburg.

¹ W. Bao *et al.*, *Phys. Rev. Lett.* **71**, 766 (1993).

² W. Bao, C. Broholm, J. M. Honig, P. Metcalf, and S. F. Trevino, *Phys. Rev. B* **54**, R3726 (1996); W. Bao *et al.*, *Phys. Rev. Lett.* **78**, 507 (1997).

³ S. A. Werner, personal communications.

⁴ S. Langenbuch, M. W. Pieper, P. Metcalf, and J. M. Honig, *Phys. Rev.* **53**, R472 (1996); M. W. Pieper, habilitation, Universität Hamburg, 1997.

⁵ A. Georges, G. Kotliar, W. Krauth, and M. J. Rozenberg, *Rev. Mod. Phys.* **68**, 13 (1996).

⁶ I. Nebenzahl and M. Weger, *Phil. Mag.* **24**, 1119 (1971); J. Ashkenazi and T. Chuchem, *Phil. Mag.* **32**, 763 (1975).

⁷ L. F. Mattheiss, *J. Phys.: Condens. Matter* **6**, 6477 (1994).

⁸ J. C. Slater and G. F. Koster, *Phys. Rev.* **94**, 1498 (1954).

⁹ A. W. Overhauser, *Phys. Rev.* **128**, 1437 (1962).

¹⁰ P. A. Fedders and P. C. Martin, *Phys. Rev.* **143**, 245 (1966).

- ¹¹ W. Young, *J. Phys. F: Metal Phys.* **5**, 2343 (1975);
W. Young, *J. Phys. F: Metal Phys.* **6**, 829 (1976).
¹² A. V. Chubukov and K. A. Musaelian, *Phys. Rev. B* **51**,
12605 (1995).
¹³ J. Appel and A. W. Overhauser, *Phys. Rev. B* **18**, 758
(1978).
¹⁴ S. A. Carter, T. F. Rosenbaum, J. M. Honig, and J. Spalek,
Phys. Rev. Lett. **67**, 3440 (1991); S. A. Carter *et al.*, *Phys.*
Rev. B **49**, 7898 (1994).
¹⁵ D. B. McWhan, A. Menth, J. P. Remeika, W. F. Brinkman,
and T. M. Rice, *Phys. Rev. B* **7**, 1920 (1973).
¹⁶ A. Bardasis and J. R. Schrieffer, *Phys. Rev. Lett.* **7**, 79
(1961).
¹⁷ G. A. Thomas, D. H. Rapkine, S. A. Carter, A. J. Millis,
T. F. Rosenbaum, P. Metcalf, and J. M. Honig, *Phys. Rev.*
Lett. **73**, 1529 (1994).
¹⁸ T. M. Rice, *Phys. Rev. B* **2**, 3619 (1970).
¹⁹ A. W. Overhauser, *J. Phys. Chem. Solid* **13**, 71 (1960).
²⁰ S. A. Werner, *Comments Cond. Mat. Phys.* **15**, 55 (1990).
²¹ K. Binder and A. P. Young, *Rev. Mod. Phys.* **58**, 801
(1986); P. W. Anderson, *Phys. Today*, March 1988, p. 9.

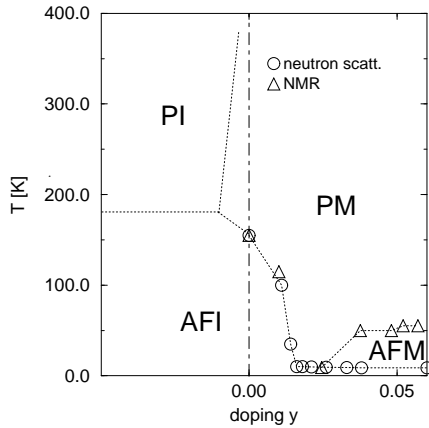


FIG. 1. Phase diagram of $V_{2-y}O_3$ as derived from neutron scattering, susceptibility, and NMR measurements. PM: paramagnetic metal, AFI: antiferromagnetic insulator, AM: antiferromagnetic metal, PI: paramagnetic insulator.

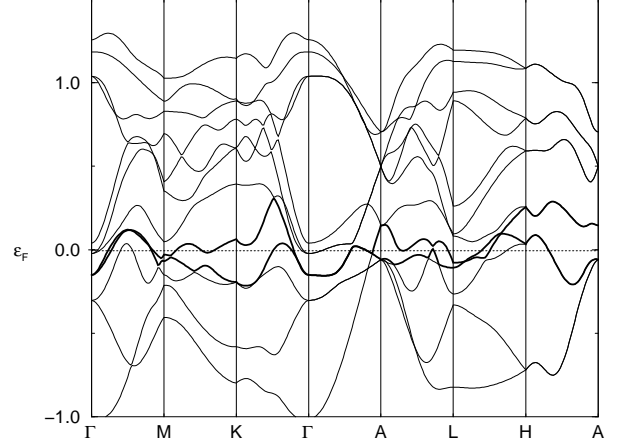


FIG. 2. Bandstructure in the vicinity of the Fermi energy ($\epsilon = 0$) plotted along lines of high symmetry of the hexagonal-type Brillouin zone.

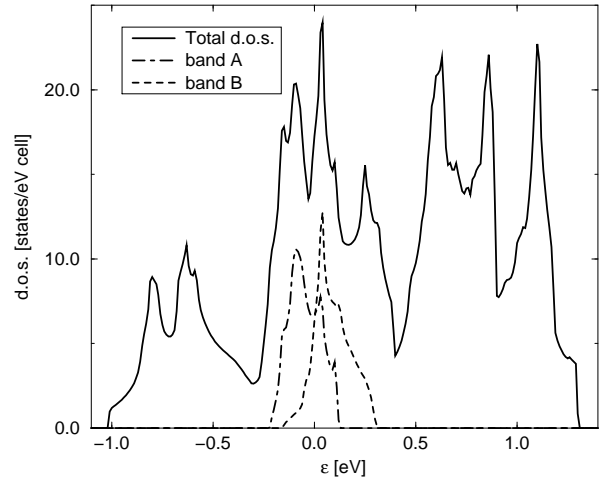


FIG. 3. Total density of states near the Fermi energy and partial density of states for the two bands, that contribute most at the Fermi energy.

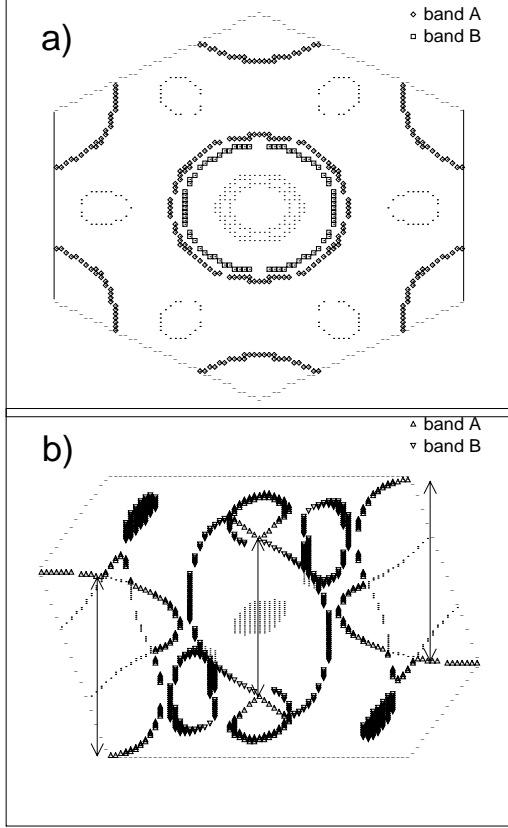


FIG. 4. Fermi surface in the Brillouin zone of V_2O_3 . a) Plot in the k_x - k_y -plane ($k_z=0$). b) k_x - k_z -plane ($k_y=0$). The arrows indicate regions of parallel Fermi surface sheets of band A connected by the numerically determined nesting vector \mathbf{Q} .

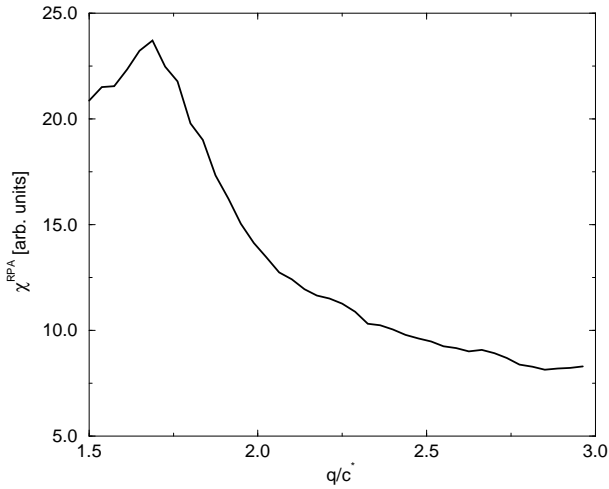


FIG. 5. The RPA susceptibility for $U = 0.4$ eV without any quasi-particle scattering in the paramagnetic state just above the SDW transition. Other values of q/c are accessed using the periodicity and the inversion symmetry of the lattice.

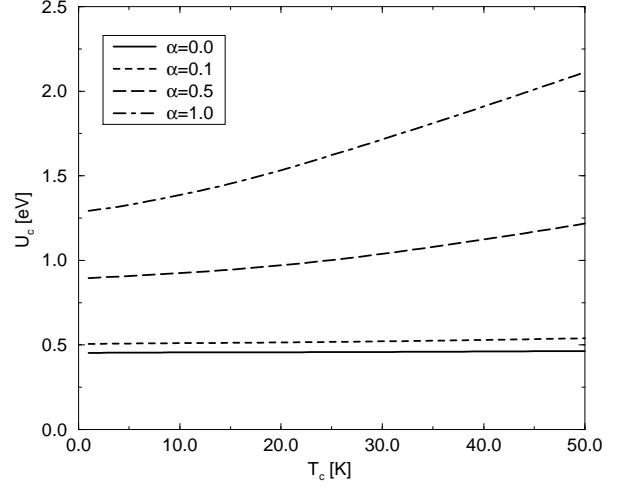


FIG. 6. Critical interaction necessary to achieve a given T_N . The electron-electron parameter α determining the scattering strength is explained in the text.

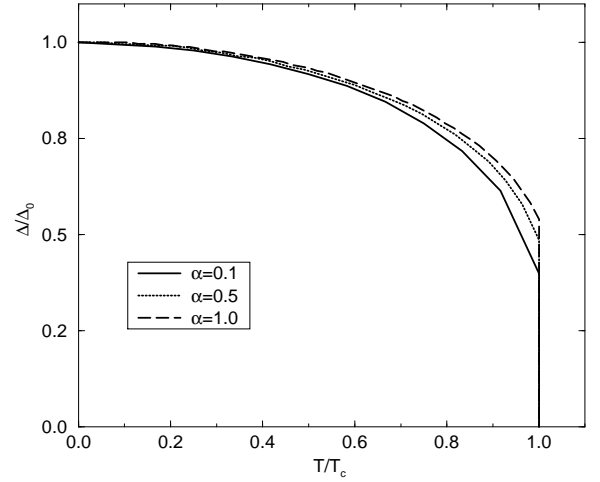


FIG. 7. Order parameter $\Delta(T)$ plotted against reduced temperature T/T_N for different strengths of quasi-particle scattering.